# Synthesis and electrochemical characterization of Si/$TiO_2$/Au composite anode: efficient oxygen evolution and hydroxyl radicals generation

G. G. Bessegato[a,b,c,1*], M. D. Cooke[b], P. A. Christensen[c], D. Wood[b,2], M. V. B. Zanoni[a]

[a]*São Paulo State University (Unesp), Institute of Chemistry, Araraquara, São Paulo, 14800-060, Brazil*

[b]*Department of Engineering, Durham University, Durham, DH1 3LE, U.K.*

[c]*School of Engineering, Newcastle University, Newcastle upon Tyne, NE1 7RU, U.K.*

**Corresponding author: guilherme.bessegato@unioeste.br; guilhermebessegato@gmail.com*

*Present addresses:*

[1] *Interdisciplinary Research Group on Environmental Photochemistry and Electrochemistry, Western Parana State University (Unioeste), Toledo, Paraná, 85903-000, Brazil*

[2] *Smart Materials and Surfaces Group, Department of Mathematics, Physics and Electrical Engineering, University of Northumbria, Newcastle upon Tyne, NE1 8ST, U.K.*

**Abstract**

This paper describes the photoelectrochemical properties of a novel composite anode composed of a 200 nm Au-Sb ohmic contact/300 μm n-Si wafer/20 nm $TiO_2$ /120 nm Au grid. By connecting the Au ohmic contact to the gold grid via a power supply, holes thermally or photochemically generated in the Si are launched to the $TiO_2$ surface where they are converted to •OH radicals. We show that the Si/$TiO_2$/Au composite anode can be efficiently employed in the oxygen evolution reaction and prove that the anode generates hydroxyl radicals (using *p*-nitrosodimethylaniline as a probe). Potential applications include the photoelectrocatalytic oxidation of organic contaminants, water splitting, and organic electro-synthesis.

**Keywords:** photoelectrochemistry, titanium dioxide, oxygen generation, dye degradation.

## 1 Introduction

The development of new photocatalytic materials, with improved properties and potentially wide application, has attracted increasing attention, particularly amongst researchers interested in $TiO_2$ [1,2]. $TiO_2$ is one of the most researched semiconductors due to properties such as stability, low cost and the surface redox reactions involving holes and electrons [3,4]: for example, the use of $TiO_2$ in the photoelectrocatalytic treatment of organic pollutants is well known [3,5,6]. This relies on the generation of hydroxyl radicals ($^{\bullet}OH$) from $H_2O/OH^-$ by holes photogenerated in the $TiO_2$ valence band (VB), which are strongly oxidizing. However, due to its high band gap ($E_g$ = 3.0~3.2 eV), the material is photoexcited only under UV irradiation (less than ~400 nm) [3,4]. This corresponds to a narrow range (≈ 7%) of solar light, which could be a free source of energy [4]. Moreover, electron−hole recombination (which reduces the lifetime of charge carriers) limits the quantum yield of $TiO_2$ significantly [7].

Various strategies have been implemented to enhance the lifetimes of the charge carriers in $TiO_2$ and move its photoexcitation into the visible region of the solar spectrum [3,8,9]. In this context, the preparation of semiconductor heterojunctions is well known in the photoelectrochemical field [10,11]. In this strategy, the coupling of two semiconductors with a clear energy disparity between their valence and conduction bands leads to electron and hole transfer between the two materials in opposite directions, thus minimizing charge carrier recombination. In addition, this approach can result in excitation by visible light if one of the semiconductors has a suitably small band gap energy [12]: hence the combination of $TiO_2$ with silicon has been investigated [13–17] and the combination has been shown to have different charge transport dynamics, to be capable of visible light excitation and to have controllable conductivity.

Monocrystalline silicon finds wide applications in both the electronics industry and in photovoltaics [18]. It also has a relatively small band gap ($E_g$ = 1.12 eV) meaning that electron/hole pairs are generated by irradiation with visible light or can even be thermally generated. Unfortunately, the holes do not have enough energy to oxidize water to $^{\bullet}$OH, due to the low valence band potential (+0.5 V *vs* SHE) [19,20]; in addition, Si slowly corrodes in water [19]. If compatible, a heterojunction of $TiO_2$ and silicon (n-n semiconductor heterojunction, type I, straddling gap) could provide a stable material capable of the photogeneration of hydroxyl radicals with visible light, and this was indeed suggested by previous studies on n-Si/$TiO_2$/Au composite anodes [13,21]. It was postulated that holes thermally generated in the Si could be accelerated to the surface of the $TiO_2$ by a bias voltage, $V_b$, between the positively charged Si and negatively charged Au grid, and produce $^{\bullet}$OH radicals via a reaction with water. A similar electrode, utilising a p-type silicon wafer, was found to selectively reduce $CO_2$ to ethanol [14].

Although the combination of $TiO_2$ with silicon could provide a stable material with a visible light response and good performance as photocatalyst and electrocatalyst, its applicability in water oxidation reactions and oxygen evolution is still a challenge. Since the pioneering work of Fujishima and Honda, the photo-assisted electrolysis of water at a metal oxide semiconductor surface has attracted much attention [22]. The photoelectrolysis of water generates oxygen at the photoanode and hydrogen at the cathode: however, the reaction at the photoanode is associated with substantial energy loss, mainly due to high oxygen overpotentials [23]. This could be overcome by the possibility of launching holes thermally or photochemically generated in the Si to the $TiO_2$ by the assistance of a bias voltage, allowing water oxidation at lower electrochemical potentials. The work reported in this paper shows that the Si/$TiO_2$/Au heterojunction can combine (i) an electrochemical potential and a voltage bias simultaneously, (ii) the stability and oxidizing capabilities of $TiO_2$ and (iii) the

low silicon bandgap, to produce a powerful anode. Some techniques of microfabrication are needed for the deposition of the gold grid in the design of a grid; however, this design is that allows the complex electrochemistry behaviour at the gold, at the same time permitting radiation reaching the semiconductors for the generation of electron/hole pairs. The investigation of its electrochemical and photo(electro)chemical properties is a new proposal of oxidative electrochemistry with a wide range of potential applications. A new approach of application is investigated dealing with oxygen evolution reaction and hydroxyl radicals photogeneration, which is used to oxidize a *p*-nitrosodimethylaniline probe.

## 2 Experimental

### *2.1 Preparation of the Si/$TiO_2$/Au composite anode*

The Si/$TiO_2$/Au composite anodes were composed of a silicon wafer substrate (n-type phosphorus-doped, 10-30 Ω cm, {100} orientation, 300 ± 10 μm thickness), with a 20 nm layer of $TiO_2$ deposited on one surface via atomic layer deposition (ALD; Ultratech Savannah 2) and an Au grid deposited on top of the $TiO_2$ by photolithography and lift-off techniques, using the methodology described below and summarized in Figure S1.

The Si wafer substrate was carefully cleaned in a $H_2O_2$:$H_2SO_4$ (1:3) solution for 30 min, then washed with deionized water (18 MΩ cm) and immersed in 3 M aqueous HF (10% HF in DI water) for 2 min (until all the oxide was removed). The Si wafer was then rinsed in deionized water and carefully dried using filtered $N_2$ flow.

The $TiO_2$ layer was deposited onto the Si wafer, after which the wafer+$TiO_2$ was annealed at 450 °C for 30 min in a $N_2$ flow to convert the amorphous $TiO_2$ to the anatase phase [24]. A 200 nm-thick ohmic contact comprising Au (99%) and Sb (1%) was deposited on the face of the Si wafer without the $TiO_2$ layer using a thermal evaporator (Edwards 306 Coater) and

alloying of the contact promoted by heating at 400 °C for 15 min in a $N_2$ flow. Using the same coater, a 200 nm-thick Au layer was deposited on the Au/Sb layer. The composite wafer was then dehydrated at 160 °C for 10 min on a heating plate and two different photoresists (SF9 and SPR350) were spin-coated sequentially and baked at 160 °C for 3 min and 110 °C for 3 min, respectively.

To generate the grid pattern for the deposition of the Au on the $TiO_2$ layer, the sample was placed in a mask aligner and exposed to UV light for 85 mJ $cm^{-2}$. The grid pattern was developed in a solution of MF319 developer for 50 s and baked at 160 °C for 3 min. The sample was again exposed to the MF319 developer for 180 s and rinsed with deionised water. A Cr seed layer (10 nm) was thermally evaporated for better grid adhesion on $TiO_2$, followed by a 120 nm-thick Au layer. The grid was produced by lifting off the photoresist in NMP at 70 °C, followed by final cleaning in acetone, isopropanol, and deionized water. The gold grid was 375 μm wide with an open area of 1 $mm^2$ for each periodic repeat unit. This construction is similar to those reported previously [13,21], and a typical SEM image of the grid is shown in Figure 1.

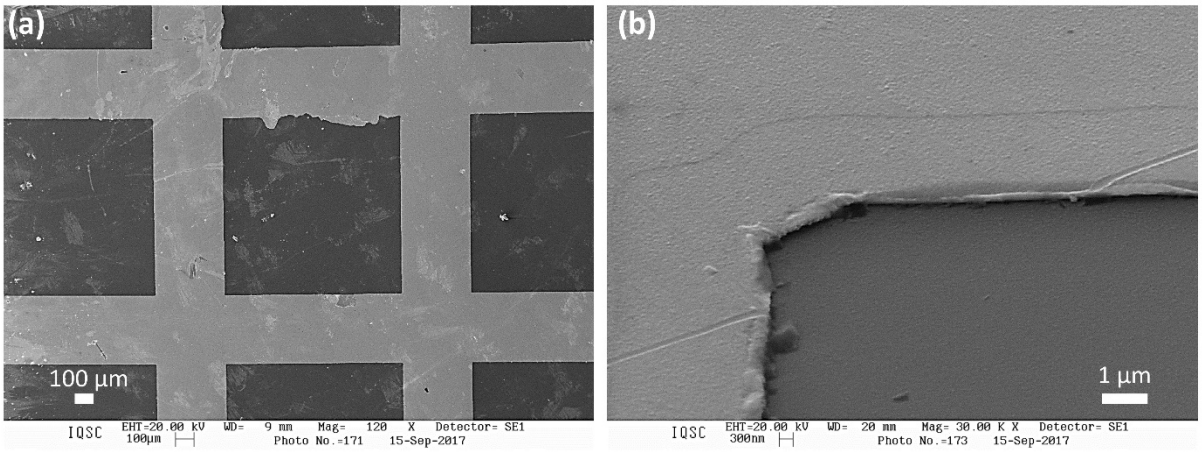


**FIG.1**

Finally, the circular composite samples (Figure 2) were cut into four pieces using a wafer scribe. The electrical contacts comprised two thin wires electrically attached onto the gold grid using silver epoxy (RS silver loaded epoxy adhesive/hardener system) and the epoxy allowed to harden overnight, after which the epoxy areas were covered with a layer of Araldite Rapid resin. On the back contact, a thick wire was attached using the same procedure, and this entire surface was covered with Araldite Rapid, such that only the Au grid and $TiO_2$ could be in contact with the electrolyte. Using a multimeter, the resistance between the front contacts was found to be 1.6 Ω and the resistance between the back and front contacts was 130 Ω. Figure S2 shows photographs of the composite anode and a schematic of its structure.

### *2.2 Characterisation of the Si/$TiO_2$/Au composite anode*

#### *2.2.1 Current/voltage characteristics of the Si/$TiO_2$/Au electrode in air and in aqueous solution*

Current/voltage ($I/V$) plots of the sample were obtained in the dark and under visible light irradiation (Cole Parmer 9741-52 low-noise fibre optic illuminator equipped with a halogen lamp, emission range 400–1000 nm). The front grid contacts were connected to the working electrode input, and the back contact was connected to the counter and reference inputs of an Autolab PGSTAT12 potentiostat according to Figure S3(b). The voltage difference between front and back contacts is defined as the 'bias voltage', $V_b$, and the resultant measured current as the 'bias current', $I_b$. The anode was clamped (grid uppermost) and a light pipe from the illuminator was positioned directly above to irradiate the anode through 5 cm of water in a Pyrex beaker as a heat filter (see Figure S3). This arrangement was maintained for all measurements to ensure the distance from the end of the light pipe to the gold grid did not

alter. All experiments were conducted at 25 °C, and the solutions employed were: Milli-Q water (18.2 MΩ cm), 0.01 M $Na_2SO_4$, 0.01 M NaOH, and 0.01 M $H_2SO_4$.

### *2.2.2 Photocurrent measurements at open circuit*

In the context of this work, open circuit referred to experiments conducted without an applied potential $E_{ec}$. The grid side of the composite anode was irradiated and the photocurrent ($I_{hv}$) and photovoltage ($V_{hv}$) between the front and back contacts measured, see Figure S4, using two digital voltmeters. The photocurrent, $I_{hv}$, is equal to the current measured under irradiation minus the current in the dark ($I_{hv} = I_{light} - I_{dark}$). Nine different intensities of light were used to irradiate the anode via the iris on the fibre optic illuminator. Using a light meter (RS, model 180-7133), illuminance (density of luminous flux on the electrode surface in lumens/area or lux) of all the different intensities was measured before starting the experiments. $I_{hv}$ and $V_{hv}$ were measured using DI water and $1\times10^{-5}$ M, $1\times10^{-4}$ M, $1\times10^{-3}$ M and $1\times10^{-2}$ M $H_2SO_4$, $Na_2SO_4$ and NaOH. After each experiment in a specific medium, the anode was rinsed in DI water and dried in flowing nitrogen. The data refers to the average of identical experiments conducted three times.

### *2.2.3 Cyclic voltammetry*

The voltammetric behaviour of the composite anode was investigated by employing it as the working electrode, gold grid face down, in a standard three-electrode cell, see Figure 2. The electrochemical potential, $E_{ec}$, of the gold grid of the composite anode was maintained with respect to a Ag/AgCl (KCl 3 M) reference electrode, which was employed via a Luggin capillary held close to the gold grid face of the composite anode working electrode. A Ti/Pt mesh (6 $cm^2$) counter electrode was positioned parallel to the gold grid and below the

working electrode. Cyclic voltammetry measurements were taken in 0.5 M $H_2SO_4$ electrolyte at a scan rate of 100 mV $s^{-1}$ using an Autolab PGSTAT12 potentiostat.

The Au grid was biased negative relative to the Au ohmic contact of the Si wafer via a 9 V-12 Ah sealed lead acid battery (Maplin) as shown in Figure 2: a battery was chosen as a dc power supply to avoid complications due to earth loops. As stated above, the bias voltage between the gold grid and Ohmic contact is denoted as $V_b$, and the corresponding bias current is $I_b$.

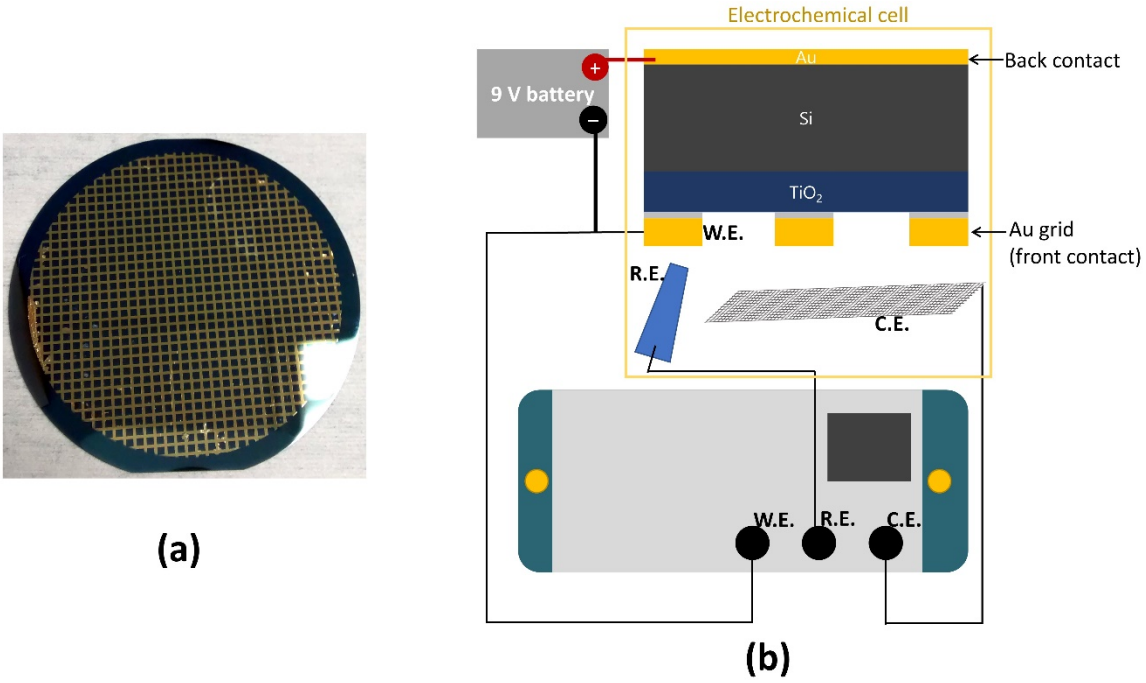


**FIG.2**

### *2.3 Oxygen measurements*

Oxygen generation by the Si/$TiO_2$/Au composite anode was carried out in a glass cell capable of isolating the interior compartment from the environment. The composite anode, the counter, and reference electrodes, the oxygen sensor, and a glass tube to bubble $N_2$ were inserted through the lid of the cell, see Figure S5. The oxygen sensor was a Clark membrane

electrode (AZ Instruments, model AZ8403). The cell was sealed using plastic adhesive. Before starting the experiments, the electrolyte (0.5 M $H_2SO_4$) was purged with $N_2$ until the minimum $O_2$ concentration was obtained. The cell was placed above a magnetic stirrer and was illuminated from beneath. The concentration of dissolved oxygen was measured during three different conditions: i) under bias voltage, $V_b$ = 1.2 V; ii) electrochemical potential, $E_{ec}$ = 0.95 V and $V_b$ = 1.2 V; and iii) $E_{ec}$= 0.95 V and $V_b$ = 1.2 V under visible light irradiation.

### *2.4 Detection of hydroxyl radicals*

The spin trap *p*-nitrosodimethylaniline (RNO) was employed to detect •OH radicals. The RNO is selectively oxidized by •OH radicals, (the exact reaction mechanism of which is still unclear) and the bleaching of the strong absorption band at 440 nm was followed by UV/vis spectrophotometry [25,26].

A quartz beaker was employed as a photoelectrochemical cell, irradiated through its base by visible light from a Newport Corporation simulator with an AM 1.5G filter, equipped with a xenon arc lamp of 300 W. A beaker with water between the light output and the PEC cell was used as a heating filter. The composite anode was the working electrode, with an Ag/AgCl (KCl 3 M) reference and a Ti/Pt mesh counter electrode positioned parallel below the working electrode (Figure S6). The concentration of the RNO was 2.2 mg $L^{-1}$ in 0.5 M $H_2SO_4$ and its absorbance was monitored at 440 nm using a 1 cm pathlength cuvette in an Agilent Cary 60 spectrophotometer. Three experiments were used in order to evaluate •OH generation: i) under $V_b$ = 1.2 V; ii) $E_{ec}$ = 0.95 V and $V_b$ = 1.2 V; and iii) $E_{ec}$= 0.95 V and $V_b$ = 1.2 V under visible light.

## 3 Results and discussion

### *3.1 Current/Voltage characteristics of the Si/TiO₂/Au composite anode*

IV curves (here referred as $I_b/V_b$ plots) shows the relationship between the voltage applied across an electrical device and the current flowing through it. There is interest in the mechanism of charge carriers (electrons and holes) transport through the heterojunction composite anode when submitted to forward and reverse bias conditions. At this point, there is no particular interest in the electrochemical behaviour of the electrode surface (which will be obtained by the voltammetric analysis).

Figure 3 shows $I_b/V_b$ plots for a Si/$TiO_2$/Au composite anode in air, and with a layer of Milli-Q water, 0.01 M $Na_2SO_4$, NaOH and $H_2SO_4$; in all cases, both in the dark and under irradiation from a visible light lamp (see Figure S3). The Au grid was biased in a negative direction with respect to silicon. At $V_b = 0.0$ V in the dark, $I_b$ was zero under all conditions. At $V_b < 0.0$ V, the observed bias current was due to the hole transport from Si to $TiO_2$.

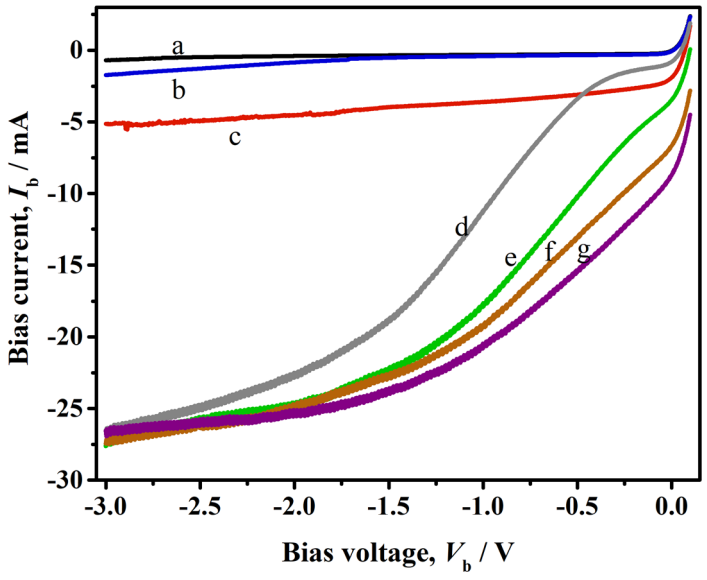


**FIG.3**

As can be seen from plots (a) and (b) in Figure 3, in the dark with and without a layer of water, the bias current increases from zero as $V_b$ is made increasingly negative before remaining essentially constant. Under irradiation in air, the form of the plot is essentially the same as in the dark, except that there is a clear photocurrent ($I_{hv}$, the difference between the two plots) at $V_b = -3$ V is ~5 mA. In the presence of all aqueous layers, the photocurrents are significantly increased over that observed in air and the plots show a markedly different structure in that $I_b$ does not simply increase then attain a plateau. All the plots obtained using an aqueous layer show an inflexion between ~0 and 0.5 V, and this inflexion moves towards increasingly negative $V_b$ as the pH of the aqueous layer moves from alkaline to acidic: however, all these plots show approximately the same bias current at $V_b = -3$ V. The water filter ensured that the lamp did not heat the anode, so the increased currents and changes in $I_b/V_b$ response must be due to photogeneration of electrons and holes in the Si and the injection of the latter into the $TiO_2$ and their reaction with aqueous species at the $TiO_2$ surface. Assuming that the number of photons reaching the anode is the same in all the solutions, then the same number of electron/hole pairs are presumably generated: the very marked difference between the experiments in air and with the aqueous layers strongly suggests that the carriers are not properly "separated" without the presence of a receptor, such as water, on the $TiO_2$/Au surface.

The pH dependence of the plots obtained under irradiation is extremely interesting. As well as the variation in shape, but constant photocurrent at −3 V, there is a marked difference in the bias currents observed at $V_b = 0.0$ V: thus the bias currents observed at $V_b = 0.0$ V were 0.9, 1.9, 3.5, 6.6, and 8.7 mA for $H_2SO_4$, air, water, $Na_2SO_4$, and NaOH, respectively. This will be discussed in the next section.

### *3.2 The dependence of the photocurrent on pH and light intensity*

Figure 4(a) shows the graph of photocurrent ($I_{hv}$) at $V_b$ = 0.0 V *vs* illuminance for a Si/$TiO_2$/Au composite anode under nine different light intensities in air, and with a layer of water, and 1.0 × $10^{-2}$ M $H_2SO_4$, $Na_2SO_4$ and NaOH.

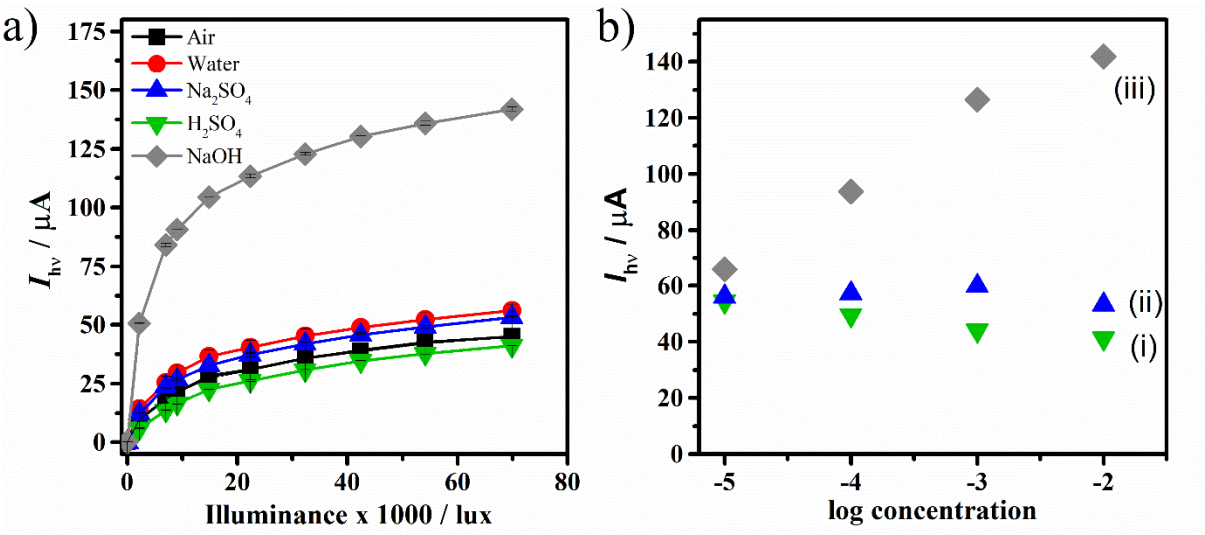


**FIG.4**

Leaving the experiment using NaOH aside for the time being, there is only a slight dependence of the photocurrent on pH, or the presence/absence of an aqueous layer: at a light intensity of 7 × $10^4$ lux $I_{hv}$ was between 41–56 μA; being the smallest $I_{hv}$ from acidic layer and the highest from neutral layers (water and $Na_2SO_4$ aqueous solution). However, when covered with 0.01 M NaOH, a photocurrent of 150 μA was observed, ~3.4 times higher than that observed with the other solutions or in air. Again, it appears that the photocurrent can be directly dependent on the surface reactions taking place at the $TiO_2$/electrolyte interface.

Figure 4(b) shows plots of photocurrent *vs* log concentration of $H_2SO_4$, $Na_2SO_4$, and NaOH at $V_b$ = 0.0 V. As can be seen from the figure, the responses are all linear: however, the alkaline response increases with concentration at ~26 μA per decade, the neutral solution shows little

or no dependence whilst the acidic photocurrent decreases slowly with increasing concentration.

The influence of pH on the surface charge of the titanium dioxide electrode is known [27]: thus the isoelectric point (point of zero charge, $pH_{pzc}$) of $TiO_2$ is around 5.8-7.5 in 0.01 M $KNO_3$ [28]. To illustrate this recognized feature, Figure 5 shows the protonation and deprotonation of the surface OH groups on $TiO_2$.

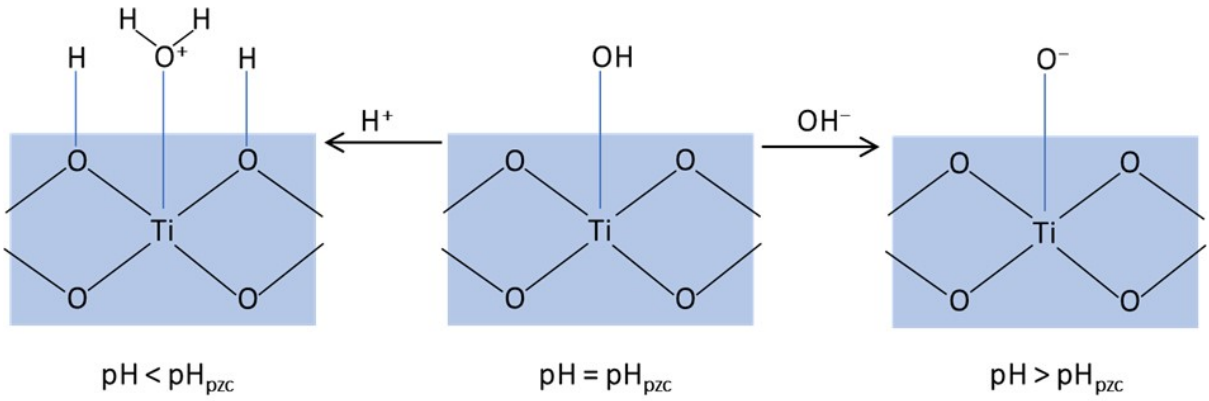


**FIG.5**

Thus, the behaviour of the photocurrent on pH suggests that the surface OH groups on the electrode in contact with electrolyte are protonated or deprotonated depending on the local pH, as described by the site-binding model [29–31]. These reactions build up a net surface charge density $\sigma_0$ and surface potential $\Psi_0$ leading to a redistribution of the ions close to the surface as described by the Boltzmann equation:

$$pH_s = pH_b + e\Psi_0/(2.3kT) \quad (1)$$

where $pH_b$ is the bulk pH and $pH_s$ the surface pH, $e$ the elementary charge, $k$ the Boltzmann constant, and $T$ the absolute temperature. According to the Boltzmann equation, a change in the bulk pH of $\Delta pH_b$ can be compensated both by a change in surface pH, $\Delta pH_s$, and a change

in the surface potential $\Delta\Psi_0$, the latter being the measured quantity. The surface hydroxyl groups are effectively buffering the surface, leading to an almost constant $pH_s$. In this case, a change in bulk $\Delta pH_b$ is fully compensated by the surface potential and the so-called Nernstian response $\Delta\Psi_0 = 2.3kT/e\Delta pH_b = 59.5$ mV/pH (at room temperature) is observed (this response depends on the oxide properties, and it is not always Nernstian) [29,32]. Thus, in Figure 4(b), by changing [NaOH] or [$H_2SO_4$] the photocurrent (related to photovoltage by Ohm's law) is changed accordingly. However, as $Na_2SO_4$ is pH inactive, it does not affect the photocurrent at open circuit.

Similar behaviour was reported by Pu and colleagues [33], investigating the key aspects related to surface states of $TiO_2$ nanotubes in solutions at different pH values. In acidic medium, they found that $TiO_2$ nanotubes electrode has a very narrow space charge region, whereas the contribution of surface states to the overall electronic transfer process is low. On the contrary, in alkaline solution, the presence of a high density of surface states, correlated to hydroxyl groups, provides an interesting mechanism of charge transfer mediated by these states. This mechanism could be important in photocatalytic reactions which are performed in alkaline solutions.

### *3.3 Electrochemical behaviour of the composite anode*

The electrochemical response of a Si/$TiO_2$/Au anode was investigated and the results are shown in Figure 6. The figure shows cyclic voltammograms collected using the gold grid as the working electrode in 0.5 M $H_2SO_4$ and as a function of the anodic limit. From Figure 6, it appears that Au oxide formation begins at ~ +0.5 V (*vs* Ag/AgCl) and the oxide stripping peak occurs at ~ +0.45 V. The cyclic voltammetry of $TiO_2$ is largely featureless in acid solution [34] but the shape of the voltammograms in Figure 6 are very different from those of a gold polycrystalline electrode [35,36] under the same conditions (see Figure S7). This

suggests that the $TiO_2$ is influencing the electrochemical response of the gold grid. Given the simplicity of the chemical system, the irreversible wave with an onset at $E_{ec}$ = 1.1 V is most likely due to the oxygen evolution reaction (OER), which occurs at ~1.4 V at the gold polycrystalline electrode (Figure S7):

$$O_2 + 4H^+ + 4e^- \rightarrow 2H_2O,\ E^\circ = 1.23\ V \qquad (2)$$

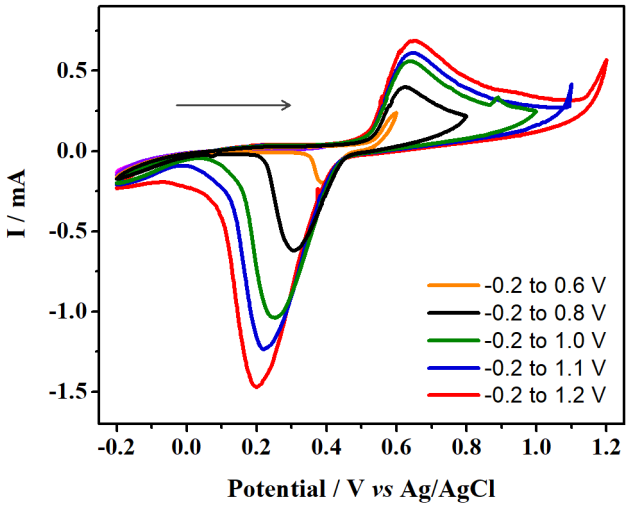


**FIG.6**

The effect of a bias voltage at an electrode potential of 1.1 V was investigated, using the system shown in Figure 2(b) and the results are presented in Figure 7. Applying bias voltages up to 0.8 V resulted in only a slight increase in the OER currents. However, at higher bias voltages, the onset potential for OER reaction decreases as $V_b$ was increased, decreasing by ~200 mV between $V_b$ = 0.8 V and 1.2 V.

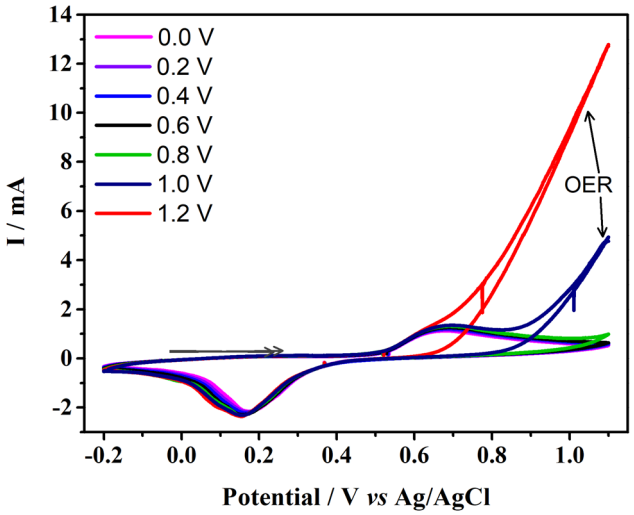


**FIG.7**

### *3.4 $O_2$ measurements*

In the experiments depicted in Figure 7 at $V_b > 0.8$V, significant gas evolution was observed at the gold grid and the counter electrode, suggesting the production of hydrogen and oxygen. In order to confirm the production of the latter at the Si/$TiO_2$/Au anode, experiments were carried out at $E_{ec}$ = 0.95 V in the dark and under irradiation at $V_b$ = 0.0 and 1.2 V using the Clark membrane electrode and the results are shown in Figure 8.

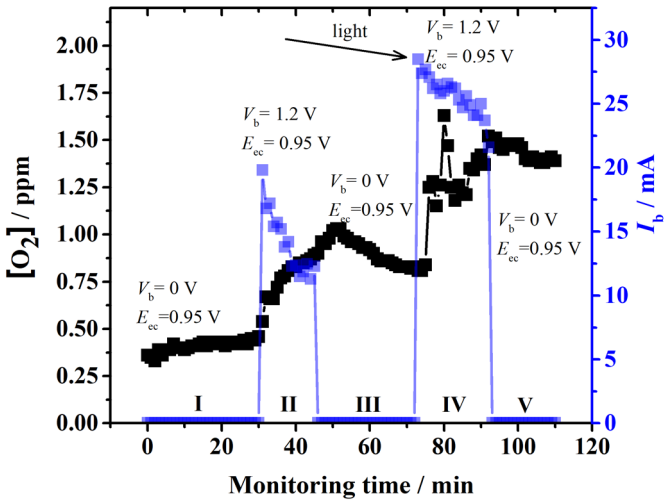


**FIG.8**

As can be seen from the figure, no oxygen was generated at $E_{ec}$ = 0.95 V and $V_b$ = 0 (Step I) as expected, as $E_{ec}$ is below its standard reduction potential ($E°$ = 1.23 V *vs* SHE). With $V_b$ = 1.2 V at the same electrochemical potential (Step II, 30–45 min) the dissolved oxygen concentration increased, reaching about 0.89 ppm (formation of ~0.50 ppm), as $I_b$ increased.

Then, $V_b$ was turned off (Step III, between 45 and 70 min), and $O_2$ level first increased and then decreased until reaching a stable value (0.81 ppm) – this condition is the same as the first step and no oxygen was generated. First, $O_2$ formed at the anode was slowly dissolved in the electrolyte increasing its concentration, and then some oxygen was partially released from the solution to establish an equilibrium. At the fourth step (70–90 min), the electrode was irradiated and $V_b$ set to 1.2 V, with a concomitant increase in dissolved $O_2$ reaching 1.52 ppm. The $O_2$ formation was about 40% higher compared to the analogous experiment in the dark, probably due to the enhanced generation of holes and electrons in the silicon layer on irradiation. The last step (Step V, 90–110 min, dark, no bias potential) showed a similar behaviour to step III, i.e. a slight increase in dissolved oxygen was observed followed by a decrease until the system reached equilibrium between gaseous and dissolved $O_2$.

The data show that even applying an electrochemical potential lower than the standard potential for oxygen evolution, the addition of a sufficient bias voltage allows the generation of oxygen and suggests that Si/$TiO_2$/Au composite anodes may offer a novel and efficient method for generating OH radicals.

Then, holes present at the $TiO_2$ surface can react with water and generate oxygen (anode half-reaction at Eq. 3), in which the steps are described in Eq. 4. The steps of oxygen generation were proposed by Rossmeisl et al. [37], in which * represents an active site on the $TiO_2$ surface. HO* species are adsorbed hydroxyl radicals, which, for convenience, can be considered as the hole carriers at the surface, and may have other fates: those which are

physically close to the gold gridlines can be captured by the gold surface, generating AuOH; or may react with oxidizable impurities [13].

$$2H_2O + 4h^+ \rightarrow O_2 + 4H^+ \quad (3)$$

$$2H_2O + h^+ \rightarrow HO^* + H_2O + H^+ + 2h^+ \rightarrow O^* + H_2O + 2H^+ + 3h^+ \rightarrow HOO^* + 3H^+ + 4h^+ \rightarrow O_2 + 4H^+ \quad (4)$$

Simultaneously to the oxygen generation by holes at $TiO_2$ surface, we need to consider the contribution of Au as well. Yang and Hetterscheid [38] reported that Au-$OH_{ads}$ would continue to convert to $Au(OH)_3$ by place-exchange reactions along further electron transfer to form a gold oxide film. Under acidic conditions, the α-oxide may be predominantly an oxyhydroxide, whose structure may include *OOH species within the oxide layer. *OOH intermediate has high energy and should rapidly decompose into $O_2$.

To the best of our knowledge, neither oxygen nor hydrogen is evolved at photoactivated naked $TiO_2$ in the absence of electron donors/acceptors and co-catalysts and assistance of an external bias potential [39,40]. In fact, oxygen can be generated by valence band holes of a $TiO_2$ photoanode (under positive bias potential) when water is oxidized, which was firstly reported by Fujishima and Honda in 1972 [22]. However, even the most efficient materials developed for water splitting are still far from the desired, as it requires the kinetically highly challenging water oxidation reaction. Several metals act as good catalysts for hydrogen evolution reaction, but there are no materials with comparable efficiency for the oxygen evolution reaction [39]. A large overpotential is necessary to drive the OER due to the sluggish four-electron transfer. Noble metal oxides, such as $RuO_2$ and $IrO_2$ are considered the benchmark catalysts to accelerate OER aiming for high production rates in both acidic and alkaline conditions [41]. Iridium oxide is usually preferred due to its higher stability and overpotential values lower than 400 mV at 10 mA $cm^{-2}$ (as low as 200 mV) [42]. It is known

that state-of-the-art non-noble metal materials for oxygen evolution reaction present high overpotential (about 330–500 mV) [43]. On the other hand, our novel composite anode has no parallels reported in the literature and could perform OER even below the standard oxygen evolution electrochemical potential when assisted by the bias voltage. The bias voltage enables a completely novel way of controlling the electrochemistry at $TiO_2$/Au surface due to the participation of thermally/photogenerated holes. Our findings are in excellent agreement with Gerischer [39,44] suggestions for the properties of an ideal semiconductor photocatalyst for the oxygen evolution reaction (OER) from water. The oxygen evolution reaction occurs at an electrochemical potential much lower than 1.23 V and overcomes the high overpotential for the oxygen evolution by electrocatalysis. In addition, the composite anode has a small band gap energy, being able to be excited by sunlight, and is more stable compared to most semiconductors with practical use under sunlight irradiation.

Due to the usually higher overpotential for OER, it is considered the bottleneck for water splitting, $CO_2$ reduction, metal-air batteries, and fuel cells, which involve oxygen evolution in their anodes. In this way, further investigation on the composite anode such as changing the morphology of gold grid to a nanostructured layer or even using a benchmark catalyst, such as $IrO_2$ or $RuO_2$, could further greatly improve the efficiency towards oxygen evolution reaction. It is why the Si/$TiO_2$/Au composite anode opens a new range of possibilities in electrochemistry.

### *3.5 Hydroxyl radicals generation*

In order to check the formation of hydroxyl radicals experiments were carried using the decolourization of *p*-nitrosodimethylaniline (RNO) dye [26,45]. The use of the organic dye *p*-nitrosodimethylaniline (RNO) is an established method for the detection of hydroxyl radicals as it is a selective spin trap for hydroxyl radicals, and does not react with singlet oxygen

($^1O_2$), superoxide anions ($O_2^-$) or other peroxy compounds [26]. The oxidative performance of Si/$TiO_2$/Au composite anode for RNO decolourization ($1.5 \times 10^{-5}$ M in 0.5 M $H_2SO_4$) was evaluated under the following conditions: i) under $V_b$ = 1.2 V in the dark, no electrochemical potential (open circuit); ii) $E_{ec}$ = 0.95 V and $V_b$ = 1.2 V, in the dark; and iii) $E_{ec}$= 0.95 V and $V_b$ = 1.2 V under irradiation (300 W Xenon lamp with an AM 1.5G filter) (see Figure 9).

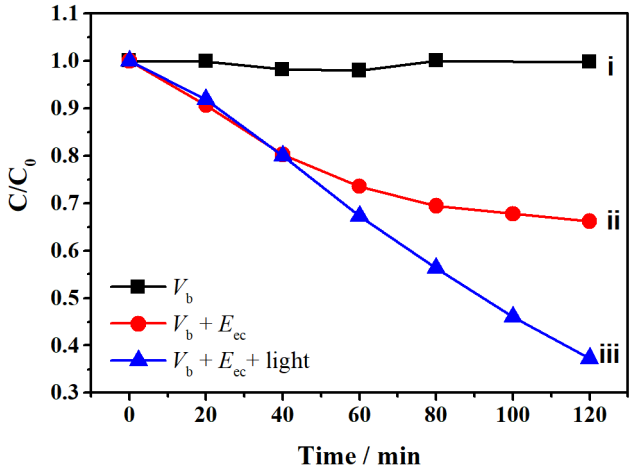


**FIG.9**

Under $V_b$, there was no oxidation (decolourization) of the RNO solution in 120 min. This observation was similar to the result obtained for oxygen generation (i.e. no oxygen evolved), and it is due to the absence of oxidizing species, such as holes or $^{\bullet}OH$ adsorbed on the anode surface. However, when an electrochemical potential is applied simultaneously to $V_b$ to the gold grid of the Si/$TiO_2$/Au anode, clear oxidation of RNO was observed, due to the generation of hydroxyl radicals at the anode surface. The decolourization was enhanced when the Si/$TiO_2$/Au photoanode was irradiated: thus Si/$TiO_2$/Au photoanodes may have the potential to be employed as an Advanced Oxidation Process in environmental treatment.

## 4 Conclusions

The characteristics of the composite anode suggest that it has unique properties especially due to the reactions that can occur at the $TiO_2$/Au surface since holes thermally generated at the silicon layer can travel to the surface under a bias voltage between the metal grid and Si. The two-dimensional control by the application of electrochemical potential and a bias voltage simultaneously open the possibility to "tune" a composite anode to oxidize a target molecule by selecting a suitable set of these parameters, and the use of visible irradiation generates more electron/hole pairs enhancing the photoelectrochemical efficiency. The presence of hydroxyl radical generation due to the holes produced at the silicon layer (thermally or photochemically) was confirmed by oxygen measurements and the oxidation of the RNO dye (probe for $^{\bullet}OH$). Then, $TiO_2$ has an important role to protect the Si substrate and, due to its more positive valence band potential, can promote water oxidation. Our composite anode represents a new area of oxidative electrochemistry and has a wide range of potential applications such as oxidative synthetic transformations and water and air detoxification.

## Acknowledgments

The authors are thankful for the financial support provided by the São Paulo Research Foundation (FAPESP) (grant numbers 2015/00822-6, 2014/03679-7, and 2012/18357-0). G.G. Bessegato is grateful for the reception of Professors D. Wood and P.A. Christensen in their laboratories.

## 5 References

[1] H. Zhang, G. Chen, D.W. Bahnemann, Photoelectrocatalytic materials for environmental applications, J. Mater. Chem. 19 (2009) 5089–5121. https://doi.org/10.1039/b821991e.

[2] Y.-C. Nah, I. Paramasivam, P. Schmuki, Doped $TiO_2$ and $TiO_2$ nanotubes: synthesis and applications, Chemphyschem. 11 (2010) 2698–2713. https://doi.org/10.1002/cphc.201000276.

[3] G.G. Bessegato, T.T. Guaraldo, J.F. de Brito, M.F. Brugnera, M.V.B. Zanoni, Achievements and trends in photoelectrocatalysis: from environmental to energy applications, Electrocatalysis. 6 (2015) 415–441. https://doi.org/10.1007/s12678-015-0259-9.

[4] I. Paramasivam, H. Jha, N. Liu, P. Schmuki, A review of photocatalysis using self-organized $TiO_2$ nanotubes and other ordered oxide nanostructures, Small. 8 (2012) 3073–3103. https://doi.org/10.1002/smll.201200564.

[5] E. Mousset, · Dionysios, D. Dionysiou, Photoelectrochemical reactors for treatment of water and wastewater: a review, Environ. Chem. Lett. 1 (2020) 3. https://doi.org/10.1007/s10311-020-01014-9.

[6] X. Meng, Z. Zhang, X. Li, Synergetic photoelectrocatalytic reactors for environmental remediation: A review, J. Photochem. Photobiol. C Photochem. Rev. 24 (2015). https://doi.org/10.1016/j.jphotochemrev.2015.07.003.

[7] J. Tang, J.R. Durrant, D.R. Klug, Mechanism of photocatalytic water splitting in $TiO_2$. Reaction of water with photoholes, importance of charge carrier dynamics, and evidence for four-hole chemistry, J. Am. Chem. Soc. 130 (2008) 13885–13891. https://doi.org/10.1021/ja8034637.

[8] M. Humayun, F. Raziq, A. Khan, W. Luo, Modification strategies of $TiO_2$ for potential applications in photocatalysis: a critical review, Green Chem. Lett. Rev. 11 (2018) 86–102. https://doi.org/10.1080/17518253.2018.1440324.

[9] A.E.R. Mohamed, S. Rohani, A. El Ruby Mohamed, S. Rohani, Modified $TiO_2$ nanotube arrays (TNTAs): progressive strategies towards visible light responsive photoanode, a review, Energy Environ. Sci. 4 (2011) 1065–1086. https://doi.org/10.1039/c0ee00488j.

[10] H. Wang, L. Zhang, Z. Chen, J. Hu, S. Li, Z. Wang, J. Liu, X. Wang, Semiconductor heterojunction photocatalysts: Design, construction, and photocatalytic performances, Chem. Soc. Rev. 43 (2014) 5234–5244. https://doi.org/10.1039/c4cs00126e.

[11] O.A. Arotiba, B.O. Orimolade, B.A. Koiki, Visible light–driven photoelectrocatalytic semiconductor heterojunction anodes for water treatment applications, Curr. Opin. Electrochem. 22 (2020) 25–34. https://doi.org/10.1016/j.coelec.2020.03.018.

[12] J. Georgieva, E. Valova, S. Armyanov, N. Philippidis, I. Poulios, S. Sotiropoulos, Bi-component semiconductor oxide photoanodes for the photoelectrocatalytic oxidation of organic solutes and vapours: A short review with emphasis to $TiO_2$-$WO_3$ photoanodes, J. Hazard. Mater. 211 (2012) 30–46. https://doi.org/10.1016/j.jhazmat.2011.11.069.

[13] P.A. Christensen, M.A. Carroll, D. Linares-Moya, D. Molyneux, M.C. Rosamond, D. Wood, A novel composite anode: the electrooxidation of organic molecules via

formation of highly energetic holes, J. Phys. Chem. C. 115 (2011) 10777–10783. https://doi.org/10.1021/jp202325m.

[14] T.T. Guaraldo, J.F. De Brito, D. Wood, M.V.B. Zanoni, A new Si/$TiO_2$/Pt p-n junction semiconductor to demonstrate photoelectrochemical $CO_2$ conversion, Electrochim. Acta. 185 (2015) 117–124. https://doi.org/10.1016/j.electacta.2015.10.077.

[15] X. Yao, L. Chen, M. Liu, D. Feng, C. Wang, F. Lu, W. Wang, X. Wang, Y. Cheng, H. Liu, H. Chen, W. Wang, Rational design of Si/$TiO_2$ heterojunction photocatalysts: Transfer matrix method, Appl. Catal. B Environ. 221 (2018) 70–76. https://doi.org/10.1016/j.apcatb.2017.08.087.

[16] M. Hannula, H. Ali-Löytty, K. Lahtonen, J. Saari, A. Tukiainen, M. Valden, Highly efficient charge separation in model Z-scheme $TiO_2$/$TiSi_2$/Si photoanode by micropatterned titanium silicide interlayer, Acta Mater. 174 (2019) 237–245. https://doi.org/10.1016/j.actamat.2019.05.032.

[17] E. Coy, K. Siuzdak, M. Pavlenko, K. Załęski, O. Graniel, M. Ziółek, S. Balme, P. Miele, M. Weber, M. Bechelany, I. Iatsunskyi, Enhancing photocatalytic performance and solar absorption by schottky nanodiodes heterojunctions in mechanically resilient palladium coated $TiO_2$/Si nanopillars by atomic layer deposition, Chem. Eng. J. 392 (2020) 123702. https://doi.org/10.1016/j.cej.2019.123702.

[18] S. Sundaram, D. Benson, T.K. Mallick, Overview of the PV industry and different technologies, in: Solar Photovoltaic Technology Production, Elsevier, 2016: pp. 7–22. https://doi.org/10.1016/b978-0-12-802953-4.00002-0.

[19] Y.J. Hwang, A. Boukai, P. Yang, High density n-Si/n-$TiO_2$ core/shell nanowire arrays with enhanced photoactivity, Nano Lett. 3 (2009) 410–415. https://doi.org/10.1021/nl8032763.

[20] K. Rajeshwar, Fundamentals of semiconductor electrochemistry and photoelectrochemistry, in: A.J. Bard, M. Stratmann, S. Licht (Eds.), Encyclopedia of Electrochemistry, Wiley-VCH Verlag GmbH & Co. KGaA, 2007: p. 608. https://doi.org/10.1002/9783527610426.bard060001.

[21] P.A. Christensen, T.A. Egerton, W.F. Lin, P. Meynet, Z.-G. Shao, N.G. Wright, A novel electrochemical device for the disinfection of fluids by OH radicals, Chem. Commun. (2006) 4022–3. https://doi.org/10.1039/b608329n.

[22] A. Fujishima, K. Honda, Electrochemical photolysis of water at a semiconductor electrode, Nature. 238 (1972) 37–38. https://doi.org/doi:10.1038/238037a0.

[23] N.-T. Suen, S.-F. Hung, Q. Quan, N. Zhang, Y.-J. Xu, H.M. Chen, H.Y. Jeong, S.H. Joo, Y. Zhang, D. Wood, P. Zelenay, K. More, K. Stroh, T. Zawodzinski, J. Boncella, J.E. McGrath, M. Inaba, K. Miyatake, M. Hori, K. Ota, Z. Ogumi, S. Miyata, A. Nishikata, Z. Siroma, Y. Uchimoto, K. Yasuda, K. -i. Kimijima, N. Iwashita, Electrocatalysis for the oxygen evolution reaction: recent development and future perspectives, Chem. Soc. Rev. 46 (2017) 337–365. https://doi.org/10.1039/C6CS00328A.

[24] F. Meng, F. Lu, Characterization and photocatalytic activity of $TiO_2$ thin films prepared by RF magnetron sputtering, Vacuum. 85 (2010) 84–88. https://doi.org/10.1016/j.vacuum.2010.04.006.

[25] P. Fernández-Castro, M. Vallejo, M.F. San Román, I. Ortiz, Insight on the fundamentals of advanced oxidation processes: Role and review of the determination methods of reactive oxygen species, J. Chem. Technol. Biotechnol. 90 (2015) 796–820. https://doi.org/10.1002/jctb.4634.

[26] M.E. Simonsen, J. Muff, L.R. Bennedsen, K.P. Kowalski, E.G. Søgaard, Photocatalytic bleaching of *p*-nitrosodimethylaniline and a comparison to the performance of other AOP technologies, J. Photochem. Photobiol. A Chem. 216 (2010) 244–249. https://doi.org/10.1016/j.jphotochem.2010.07.008.

[27] M.V.B. Zanoni, J.J. Sene, M.A. Anderson, Photoelectrocatalytic degradation of Remazol Brilliant Orange 3R on titanium dioxide thin-film electrodes, J. Photochem. Photobiol. A Chem. 157 (2003) 55–63. https://doi.org/10.1016/s1010-6030(02)00320-9.

[28] R. Beranek, (Photo)electrochemical Methods for the Determination of the Band Edge Positions of $TiO_2$-Based Nanomaterials, Adv. Phys. Chem. 2011 (2011) 1–20. https://doi.org/10.1155/2011/786759.

[29] R.L. Stoop, M. Wipf, S. Müller, K. Bedner, I.A. Wright, C.J. Martin, E.C. Constable, W. Fu, A. Tarasov, M. Calame, C. Schönenberger, Competing surface reactions limiting the performance of ion-sensitive field-effect transistors, Sensors Actuators B Chem. 220 (2015) 500–507. https://doi.org/10.1016/j.snb.2015.05.096.

[30] D.E. Yates, S. Levine, T.W. Healy, Site-binding model of the electrical double layer at the oxide/water interface, J. Chem. Soc. Faraday Trans. 1 Phys. Chem. Condens. Phases. 70 (1974) 1807. https://doi.org/10.1039/f19747001807.

[31] T.W. Healy, L.R. White, Ionizable surface group models of aqueous interfaces, Adv. Colloid Interface Sci. 9 (1978) 303–345. https://doi.org/10.1016/0001-8686(78)85002-7.

[32] L. Manjakkal, D. Szwagierczak, R. Dahiya, Metal oxides based electrochemical pH sensors: Current progress and future perspectives, Prog. Mater. Sci. 109 (2020) 100635. https://doi.org/10.1016/j.pmatsci.2019.100635.

[33] P. Pu, H. Cachet, N. Laidani, E.M.M. Sutter, Influence of pH on surface states behavior in $TiO_2$ nanotubes, J. Phys. Chem. C. 116 (2012) 22139–22148. https://doi.org/10.1021/jp3060312.

[34] G.G. Bessegato, F.F. Hudari, M.V.B. Zanoni, Self-doped $TiO_2$ nanotube electrodes: a powerful tool as a sensor platform for electroanalytical applications, Electrochim. Acta. 235 (2017) 527–533. https://doi.org/10.1016/j.electacta.2017.03.141.

[35] X. Xiao, J. Ulstrup, H. Li, M. Wang, J. Zhang, P. Si, Nanoporous gold assembly of glucose oxidase for electrochemical biosensing, Electrochim. Acta. 130 (2014) 559–567. https://doi.org/10.1016/j.electacta.2014.02.146.

[36] S. Cherevko, A.R. Zeradjanin, G.P. Keeley, K.J.J. Mayrhofer, A comparative study on gold and platinum dissolution in acidic and alkaline media, J. Electrochem. Soc. 161 (2014) H822–H830. https://doi.org/10.1149/2.0881412jes.

[37] J. Rossmeisl, A. Logadottir, J.K. Nørskov, Electrolysis of water on (oxidized) metal surfaces, (2005). https://doi.org/10.1016/j.chemphys.2005.05.038.

[38] S. Yang, D.G.H. Hetterscheid, Redefinition of the Active Species and the Mechanism of the Oxygen Evolution Reaction on Gold Oxide, ACS Catal. (2020) 12582–12589. https://doi.org/10.1021/acscatal.0c03548.

[39] N. Serpone, A. V. Emeline, V.K. Ryabchuk, V.N. Kuznetsov, Y.M. Artem'ev, S. Horikoshi, Why do Hydrogen and Oxygen Yields from Semiconductor-Based Photocatalyzed Water Splitting Remain Disappointingly Low? Intrinsic and Extrinsic Factors Impacting Surface Redox Reactions, ACS Energy Lett. 1 (2016) 931–948. https://doi.org/10.1021/acsenergylett.6b00391.

[40] H.A. Vignolo-González, S. Laha, A. Jiménez-Solano, T. Oshima, V. Duppel, P. Schützendübe, B. V. Lotsch, Toward Standardized Photocatalytic Oxygen Evolution Rates Using $RuO_2$@$TiO_2$ as a Benchmark, Matter. 3 (2020) 464–486. https://doi.org/10.1016/j.matt.2020.07.021.

[41] L. Zhang, Q. Fan, K. Li, S. Zhang, X. Ma, First-row transition metal oxide oxygen evolution electrocatalysts: regulation strategies and mechanistic understandings, Sustain. Energy Fuels. 4 (2020) 5417–5432. https://doi.org/10.1039/d0se01087a.

[42] A. Touni, A. Papaderakis, D. Karfaridis, A. Banti, I. Mintsouli, D. Lambropoulou, S. Sotiropoulos, Oxygen evolution at $IrO_2$-modified Ti anodes prepared by a simple galvanic deposition method, J. Electroanal. Chem. 855 (2019). https://doi.org/10.1016/j.jelechem.2019.113485.

[43] Y. Jin, G. Xi, R. Li, Z.A. Li, X.B. Chen, T. Zhang, Nanoporous metallic-glass electrocatalysts for highly efficient oxygen evolution reaction, J. Alloys Compd. 852 (2021) 156876. https://doi.org/10.1016/j.jallcom.2020.156876.

[44] H. Gerischer, Semiconductor electrodes and their interaction with light, in: Photoelectrochemistry, Photocatalysis and Photoreactors, Springer Netherlands, Dordrecht, 1985: pp. 39–106. https://doi.org/10.1007/978-94-015-7725-0_2.

[45] J. Muff, L.R. Bennedsen, E.G. Søgaard, Study of electrochemical bleaching of *p*-nitrosodimethylaniline and its role as hydroxyl radical probe compound, J. Appl. Electrochem. 41 (2011) 599–607. https://doi.org/10.1007/s10800-011-0268-1.